Simulation of jet impingement heat transfer with the k–ε–v^2 model

By M. Behnia, S. Parneix AND P. Durbin

1. Motivation and objectives

Jet impingement heating and cooling is used in many engineering and industrial applications (e.g. materials processing, manufacturing, and cooling of computers and electronic equipment). In these applications, normally a turbulent jet of gas or liquid is directed to the target area of interest. The advantages of jet impingement heat transfer process are direct, localized heating or cooling, and increased heat fluxes. This technique is emerging as an attractive cost-effective method of cooling of computers (Nakayama 1995). There are a number of parameters to be considered in the design of such systems. For instance, for optimization of cooling or heating systems, accurate prediction of the local heat transfer coefficient is essential. To this end, the flow and thermal fields must be accurately and economically computed; hence the need for better turbulence models.

Impinging jet flows have several complex features which make them a good test vehicle for evaluation of turbulence models. In the impingement region, the mean flow is perpendicular (or nearly perpendicular) to the surface. It then turns and follows the surface in a wall jet (see Fig. 1). In the stagnation region, the flow is almost irrotational and there is a large total strain along the stagnation streamline. Away from the core of the jet, due to expansion, diffusion, and entrainment, there is substantial curvature in the streamlines. Adjacent to the wall, there are thin stagnation point and wall jet boundary layers on the target plate.

The problem of a normal impinging jet of air striking a flat plate has been considered as a test case by ERCOFTAC. They have adopted the flow and heat transfer measurements of the experiments by Cooper *et al.* (1993) and Baughn and Shimizu (1989), respectively. There are also a number of more recent heat transfer measurements by others (e.g. Baughn *et al.* 1991, Yan 1993, and Lytle and Webb 1994). The experimental data has been used by researchers to test their turbulence models for this demanding case. For instance, Craft *et al.* (1993) used the data of Cooper *et al.* (1993) and Baughn and Shimizu (1989) to examine the $k-\varepsilon$ and three second-moment closure models in an axisymmetric geometry.

The objective of our work has been to compute the flow and thermal fields in an axisymmetric isothermal fully developed turbulent jet perpendicular to a flat uniform heat flux plate using the $k-\varepsilon-\overline{v^2}$ model of Durbin (1995). To this end, the axisymmetric incompressible Navier-Stokes equations in conjunction with the standard $k-\varepsilon$, the $\overline{v^2}$ transport, and the elliptic relaxation equations have been solved on a Cartesian grid. Several turbulent Prandtl numbers and realizability constants are examined. The results are compared with the experimental data of Baughn and Shimizu (1989), Lytle (1990), Baughn *et al.* (1991), Yan (1993),

Cooper *et al.* (1993), and Lytle and Webb (1994). For comparison, computations are also performed with the widely used standard $k-\varepsilon$ model. The local heat transfer behavior of the jet for various jet to target distances is analyzed.

2. Accomplishments

2.1 The $k-\varepsilon-\overline{v^2}$ model

The mean flow satisfies the Reynolds Average Navier-Stokes (RANS) equations, where the turbulent stresses are represented with an eddy-viscosity:

$$D_t U = -\nabla P + \nabla \cdot \left\{(\nu + \nu_t)(\nabla U + \nabla^t U)\right\}$$

$$\nabla \cdot U = 0$$

The definition of the turbulent viscosity ν_t needs the evaluation of one time scale, T, and one velocity scale. For the latter, the variable $\overline{v^2}$ has been introduced by Durbin (1993a) instead of the classical turbulent kinetic energy k used in the $k-\varepsilon$ model, i.e. $\nu_t = C_\mu \overline{v^2} T$. Physically, $\overline{v^2}$ might be regarded as the velocity fluctuation normal to the streamlines; note that it is not linked to the y-component of velocity. By arguing that the physical time scale cannot be smaller than the Kolmogorov time scale, Durbin (1991) derived the following expression which prevents $1/T$ becoming infinite at the wall:

$$T' = \min(\frac{k}{\varepsilon}; 6(\frac{\nu}{\varepsilon})^{1/2})$$

Moreover, Durbin (1996) recently studied the realizability constraint in the context of impinging flows, which is our motivation here, and fixed an upper bound for this time scale:

$$T = \max(T', \frac{\alpha}{2\sqrt{3}} \frac{k}{\overline{v^2} C_\mu \sqrt{S^2}}),$$

$$\alpha \leq 1, S^2 = S_{ij} S_{ij}$$

α is a model parameter and comparison of our computations with experimental results have indicated an optimum value of 0.5 for the axisymmetric problem studied here.

Three transport equations are used for computing the turbulent kinetic energy, k, the dissipation rate of turbulence, ε, and the new velocity scale, $\overline{v^2}$:

$$D_t k = P - \varepsilon + \nabla \cdot ((\nu + \frac{\nu_t}{\sigma_k}) \nabla k)$$

$$D_t \varepsilon = \frac{C'_{\varepsilon_1} P - C_{\varepsilon_2} \varepsilon}{T} + \nabla \cdot ((\nu + \frac{\nu_t}{\sigma_\varepsilon}) \nabla \varepsilon)$$

$$D_t \overline{v^2} = k f_{22} - \frac{\overline{v^2}}{k} \varepsilon + \nabla \cdot ((\nu + \frac{\nu_t}{\sigma_k}) \nabla \overline{v^2})$$

P is the rate of production of turbulent kinetic energy, i.e. $P = 2\nu_t S^2$. It should be noted that no damping functions are used in the model equations. The k and ε equations are similar to the $k-\varepsilon$ model, except for the destruction term of ε where ε/k has been replaced by $1/T$. C'_{ε_1} has been chosen as a function of the distance to the closest boundary d in order to give suitable values of C'_{ε_1} for both turbulent boundary layer ($C'_{\varepsilon_1} = 1.55$) and plane mixing layer ($C'_{\varepsilon_1} = 1.3$), i.e. $C'_{\varepsilon_1} = 1.3 + 0.25/[1 + (d/2\ell)^2]^4$. In the channel flow or boundary layer configuration, the term kf_{22} represents the redistribution of turbulent intensity (pressure-strain correlation) from the streamwise and spanwise components. For representing non-local effects, caused by the impermeability of solid boundaries, f_{22} is evaluated through an elliptic equation (Durbin 1991):

$$f_{22} - L^2\nabla^2 f_{22} = (C_1 - 1)\frac{(2/3 - \overline{v^2}/k)}{T} + C_2\frac{P}{k}$$

Finally, by using the same approach as for the time scale (Kolmogorov length scale as a lower bound and realizability constraint for the upper bound), the following expression of the turbulent length scale can be derived:

$$L' = C_L \min(\frac{k^{3/2}}{\varepsilon}; C_\eta(\frac{\nu^3}{\varepsilon})^{1/4})$$

$$L = \max(L', \frac{1}{\sqrt{3}}\frac{k^{3/2}}{\overline{v^2}C_\mu\sqrt{S^2}})$$

The constants of the model are (Durbin 1995):

$$C_{\varepsilon_2} = 1.9, C_\mu = 0.19, C_1 = 1.4, C_2 = 0.3,$$

$$\sigma_k = 1.0, \sigma_\varepsilon = 1.3, C_L = 0.3, C_\eta = 70.0$$

2.2 Turbulent Prandtl number

In the mean temperature equation, it is customary to substitute the eddy diffusivity of heat by defining a turbulent Prandtl number, which is the ratio of the momentum to heat eddy diffusivity. There is substantial experimental data available on the turbulent Prandtl number (Pr_t). These are primarily based on determining the slope of T^+ in the log-region of a flat plate boundary layer. For air, with a molecular Prandtl number of $Pr = 0.71$, the data ranges between $Pr_t = 0.73$ and 0.92 (Kays 1994). The variation of the molecular Pr in the range of 0.7 to 64 (i.e. gases and most liquids including oils and with the exception of liquid metals) does not strongly affect the turbulent Prandtl number, and according to Kays an approximate value of 0.85 is generally acceptable.

There are also a number of analytically determined relationships for turbulent Prandtl number in the literature. Data from DNS of flow in ducts and external boundary layer flows have also been used to determine Pr_t. For instance, the DNS

results of Kim and Moin (1987) for fully developed flow of air in a duct indicate a $Pr_t \approx 1.2$ at the wall with a non-monotonic decrease to about 0.7 far from the wall. This behavior is in qualitative agreement with data based on experimental measurements in air, which according to Kays and Crawford (1993) can be represented with a relationship of the form

$$Pr_t = \frac{1}{0.5882 + 0.228(\nu_t/\nu) - 0.0441(\nu_t/\nu)^2[1 - exp(\frac{-5.165}{(\nu_t/\nu)})]}$$

This formula yields a value of 1.7 at the wall with a sharp decrease in its vicinity and an asymptotic value of 0.85 far from the wall. For the heated flat plate flow, computations of Durbin (1993b) adopting this formula and the widely used constant value of 0.9 have indicated a change of 10% in the Stanton number. In fact, these simulations have shown that the constant Pr_t value yields a marginally better agreement with experiments.

Measurements of Pr_t in other geometries (e.g. jets) are rather rare. Chua and Antonia (1990) made measurements in a circular jet of air and showed a non-monotonic variation of Pr_t between 0.84 at the axis and 1.6 near the jet edge. They suggest a constant value of 0.81 in the region between the axis and the jet half-radius point.

It is noted that there are a number of unresolved issues as far as the concept of turbulent Prandtl number is concerned (Kays 1994). Little work has been done on different geometries. Also, most of the available data is relevant to gases and there are very few measurements for higher Prandtl number liquids (e.g. dielectric liquids used for cooling of computers which have Prandtl numbers of the order of 20). Perhaps DNS of these flows can be used in the future to provide the required data for modeling.

We have examined the effect of Pr_t on the local heat transfer coefficient. We have tested several widely used Pr_t values noted above: 0.73, 0.85, 0.92, and the Kays and Crawford formula.

2.3 Available experimental data

For the turbulent impinging jet, Cooper *et al.* (1993) have recently reported a set of flow measurements at two different Reynolds numbers (i.e. $Re_D = 23,000$ and $74,000$); however, they did not make any heat transfer measurements. They note that the purpose of their experiments was to provide the hydrodynamic data for the heat transfer experiments of Baughn and Shimizu (1989) who measured the local heat transfer coefficient on a constant heat flux impingement plate. Baughn and Shimizu used a fully-developed jet striking a gold-coated plate which was painted by liquid crystals for temperature measurements and mapping of the local heat transfer coefficient. They made their measurements for several jet-to-plate spacings ($H/D \geq 2$). In a later study by Baughn *et al.* (1991), the same test rig was used to study the entrainment effects in a heated jet. They noted that their unheated jet results agreed with the earlier data of Baughn and Shimizu.

Lytle (1990) also made heat transfer and flow measurements in an impinging air jet. He used an infrared thermal imaging system for temperature measurement

and the velocity was measured by an LDV system. The focus of this study was primarily on nozzle-to-plate spacings of less than one nozzle diameter. The results have been partly published in Lytle and Webb (1994). It is noted that the relative size of the impingement plate (compared to the jet diameter) in this study was smaller than that of Baughn's experiments. Yan (1993) developed a preheated-wall transient measurement method using liquid crystals. He made local heat transfer coefficient measurements on the impingement test rig used in previous Baughn's studies. Yan notes that there was good agreement between his measurements and those of Baughn using the steady state method. Lee *et al.* (1995) also used a test rig similar to Baughn's and made measurements at lower Reynolds numbers ($Re_D < 15,000$).

2.4 Simulation results and comparison with experiments

A sketch of the problem and computational domain is shown in Fig. 1. All computations were performed using INS2D, a finite difference code in generalized co-ordinates developed at NASA Ames Research Center. The spatial discretization of convective terms was via the third order QUICK scheme. A fine, non-uniform Cartesian grid of 120×120 cells was used, with a high resolution near the solid regions (i.e. the impingement and pipe walls). A mesh sensitivity was performed by doubling the grid; however, this changed the impingement region Nusselt number by less than 0.5%. Therefore, the 120×120 grid was considered adequate. For high aspect ratios ($H/D \geq 10$), a 160 by 160 grid was used.

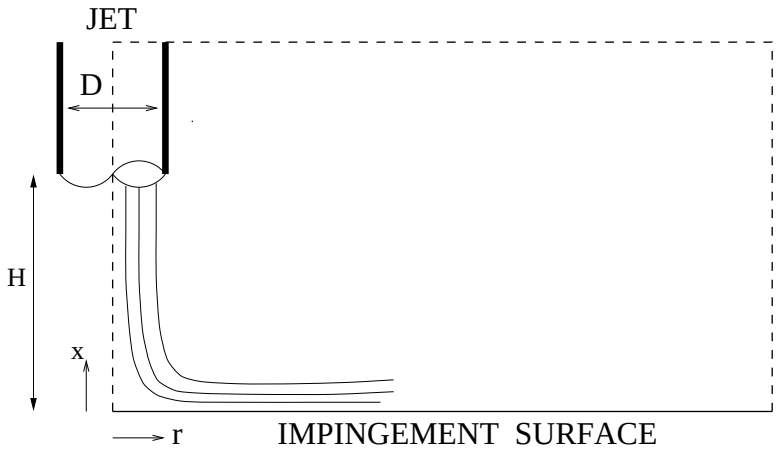

FIGURE 1. The geometry and computational domain.

The computations were performed in two steps. First, a fully-developed pipe flow simulation was performed using 240 grid points in the radial direction. For this computation, the grid spacing was chosen such that there were 5 points located in the region of $y^+ \leq 5$. This solution was then accurately interpolated and used as the inlet condition of the jet. For stability of the solution procedure and accuracy, it was necessary to include a sufficient length of pipe (of the order of 2 pipe diameters) in the computational domain; other investigators have made similar observations

(e.g. Craft *et al.* 1993). This allows the upper computational boundary to be sufficiently distanced from the wall so that it does not affect the flow near the impingement surface. Also, the effect of the jet wall thickness on the flow can be properly modeled. A specified constant static pressure condition was used for the upper and right boundaries. We examined the effect of the right boundary location on the flow and thermal fields. It was noted that once this length was larger than $(H/D+8)$, there was no noticeable effect on the flow field and local Nusselt number. For the thickness of the pipe-wall, we examined two values of 0.112D and 0.0313D corresponding to the experiments of Baughn and Shimizu (1989) and Cooper *et al.* (1993), respectively, and no noticeable difference was observed. As our main aim was comparison of the computed and measured Nusselt number, the former value was used for the computations.

Simulations were performed for a fixed jet Reynolds number of $Re_D = 23,000$ and various aspect ratios, $0.5 \leq H/D \leq 14$ using both the $k-\varepsilon$ and $k-\varepsilon-\overline{v^2}$ models. The $k-\varepsilon-\overline{v^2}$ simulations required several hundred iterations for convergence (i.e. several minutes of CPU time on the NASA - Cray C90). In general, for the $k-\varepsilon$ simulations, the number of iterations had to be doubled. For the $k-\varepsilon$ model we used a damping function of the form $\nu_t = 0.09kT[1-exp(-0.01\left|\frac{kT}{\nu}\right|)]$, which yields similar behavior to the model of Launder and Sharma (1974). Craft *et al.* (1993) used the Launder and Sharma model for the same problem and our $k-\varepsilon$ predictions are similar to theirs.

2.4.1 Preliminary computations

The effect of the realizability constraint parameter α on the computational results was determined by using two different values (i.e. 0.5 and 1). For $H/D = 2$, the computed local Nusselt number is compared with the measured data in Fig. 2a. It is noted that near the impingement region, a somewhat better agreement is obtained for $\alpha = 0.5$, however, downstream of this region and for $r/D \geq 2$, there is very little difference between the two predicted results. In this region, both values yield excellent agreement with the data. The experimental data indicate a dip in the Nusselt number around $r/D = 1.5$ with a second peak at around $r/D = 2$. This behavior seems to be better represented by the simulation with $\alpha = 0.5$, which is the value we chose to use for the computations.

The effect of the turbulent Prandtl number, Pr_t, on the local Nusselt number for $H/D = 6$ is shown in Fig. 2b. The results are not very sensitive to this parameter, in particular downstream of the impingement region. Considering the scatter in the experimental data, it is difficult to say which value of Pr_t more closely fits the data. In the stagnation region, both $Pr_t = 0.92$ and the Kays and Crawford formula are in excellent agreement with the measurements of Lytle and Webb but are slightly higher than the data of Baughn *et al.* Away from this region, as the flow becomes parallel to the plate and forms the wall jet region, the prediction with $Pr_t = 0.73$ follows the data of Baughn and Shimizu, Baughn *et al.*, and Yan. In this region, all predictions are below the measurements of Lytle and Webb. One possible explanation for the higher values of Nusselt number measured by them, in particular in this region, can be their use of a shorter length plate because of

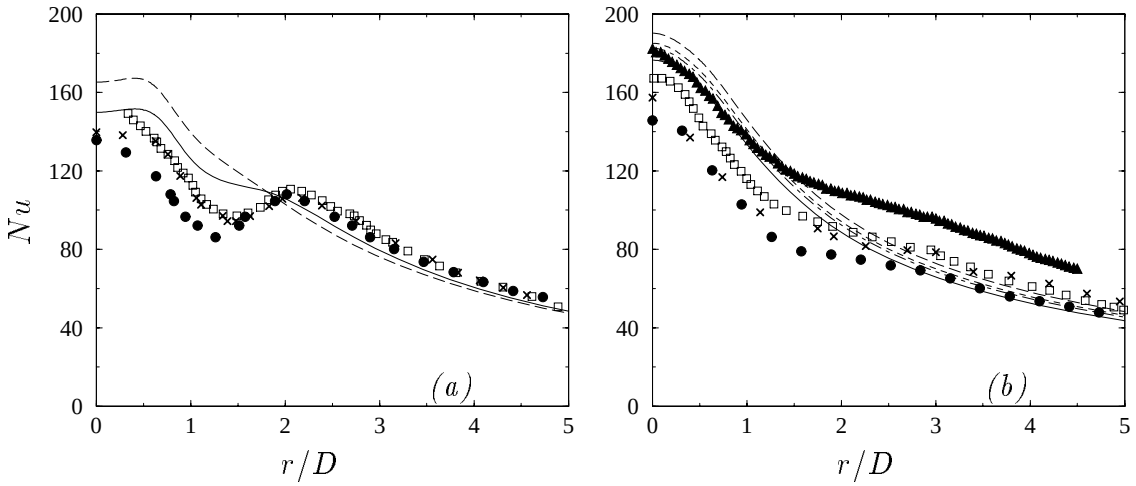

FIGURE 2. Effect of (a) the realizability constant and (b) Pr_t on the local Nusselt number; (a) $H/D = 2$ and different realizability constants, $\alpha = 0.5$ (———), $\alpha = 1.0$ (— — —); (b) $H/D = 6$ and different Pr_t, Kays & Crawford (———), $Pr_t = 0.73$ (— — —), $Pr_t = 0.85$ (·····), $Pr_t = 0.92$ (— - —). Experimental data: × Baughn & Shimizu 89 ($Re = 23750$), ▫ Baughn *et al.* 91 ($Re = 23300$), • Yan 93 ($Re = 23340$), ▲Lytle & Webb 94 ($Re = 23000$).

their interest in smaller jet to plate spacings (H/D). As the Kays and Crawford Pr_t formula yields a somewhat better agreement in the impingement region, we performed our simulations with this turbulent Prandtl number.

2.4.2 Results for $H/D = 2$

The computed flow field for this case is shown by contours of the Stokes streamlines in Fig. 3 (for clarity, only part of the domain is shown). At the nozzle exit, these are parallel to the jet axis, representing the potential core of the jet. Near the stagnation region, the flow decelerates in the axial direction and turns as exhibited by the sharp curvature in the streamlines. Past this region, and roughly for $r/D > 1.5$, a radial wall jet parallel to the plate begins to form with a developing boundary layer. The ambient fluid outside the jet is entrained into the core with a developing shear layer separating the core and the ambient fluid. The entrainment is clearly evident by the curving of the streamlines outside the pipe towards the core of the jet. This leads to the formation of a recirculation region in the vicinity of the pipe-wall (a magnified view of this region is shown as an inset in Fig. 3). The features of the flow in this region are well captured by our computations, indicating a sufficient grid resolution around the exit of the nozzle and in the shear layer.

Contours of the computed turbulent kinetic energy for both $k - \varepsilon - \overline{v^2}$ and $k - \varepsilon$ models are shown in Fig. 4. The maximum value of k predicted by the $k - \varepsilon$ model is 80% higher than that of $k - \varepsilon - \overline{v^2}$. The location of this maximum, shown by the arrows on the figure, is in the stagnation region for the $k - \varepsilon$, and at about $r/D = 2$ for the $k - \varepsilon - \overline{v^2}$. Further, the $k - \varepsilon - \overline{v^2}$ model predicts that in the shear layer between the jet core and the outer entrainment region, there exists a region of high turbulent kinetic energy. The behavior predicted by the $k - \varepsilon - \overline{v^2}$

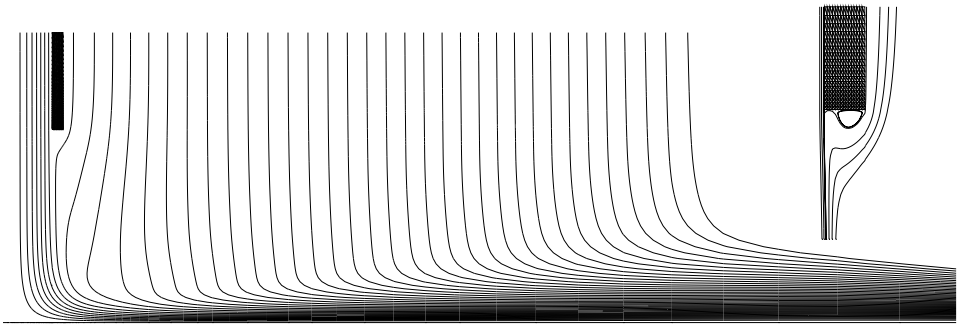

FIGURE 3. Streamlines for $H/D = 2$ computed with the $k - \varepsilon - \overline{v^2}$ model (inset shows the magnified view of the flow near the pipe exit).

model is qualitatively confirmed by the measurements of Lytle and Webb, who also noted an increase in the turbulent intensity away from the stagnation region. They attribute this to the interaction of the accelerating radial flow with the free-stream air. However, our computations suggest that it is due to increased production in the region of streamline convergence.

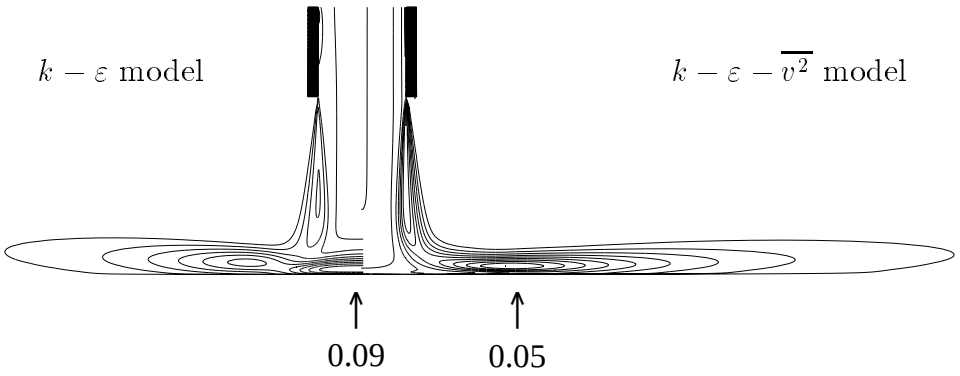

FIGURE 4. Contours of turbulent kinetic energy for $H/D = 2$.

For this aspect ratio, Craft *et al.* 1993 have made velocity measurements at various radial locations (this data was obtained from the ERCOFTAC 1996 database). A comparison of the measured velocity magnitude and our computations with the $k - \varepsilon$ and $k - \varepsilon - \overline{v^2}$ models at four different radial locations are shown in Fig. 5. On the stagnation streamline ($r/D = 0$) there is very little difference between the two predictions, and quite good agreement with the experimental data is noted. At $r/D = 0.5$ the $k - \varepsilon$ model predicts lower velocities than the $k - \varepsilon - \overline{v^2}$, which yields a somewhat better agreement near the wall. However, at this radial location away from the wall, for $x/D \leq 0.25$, the $k - \varepsilon$ predictions are closer to the experimental value, whereas in the outer region, the $k - \varepsilon - \overline{v^2}$ exactly follows the data. In the wall jet region, at $r/D = 1$, the $k - \varepsilon - \overline{v^2}$ model correctly predicts the flow acceleration, and there is excellent agreement with the data near the wall and a slight over-prediction in the outer region. At this radial location, the $k - \varepsilon$ model predicts low velocities in the wall region and high velocities in the outer region. Further

downstream, the flow decelerates, and again the $k-\varepsilon-\overline{v^2}$ model correctly predicts this behavior with a very good agreement with the experiment at $r/D = 2.5$. The $k-\varepsilon$ model does not correctly resolve the development of the boundary layer, leading to an under-prediction of the velocity in the wall region and an over-prediction in the outer region. The failure of the $k-\varepsilon$ model to correctly resolve the behavior of the flow is, perhaps, at least partly due to its prediction of high levels of turbulent kinetic energy in the stagnation region (see Fig. 4).

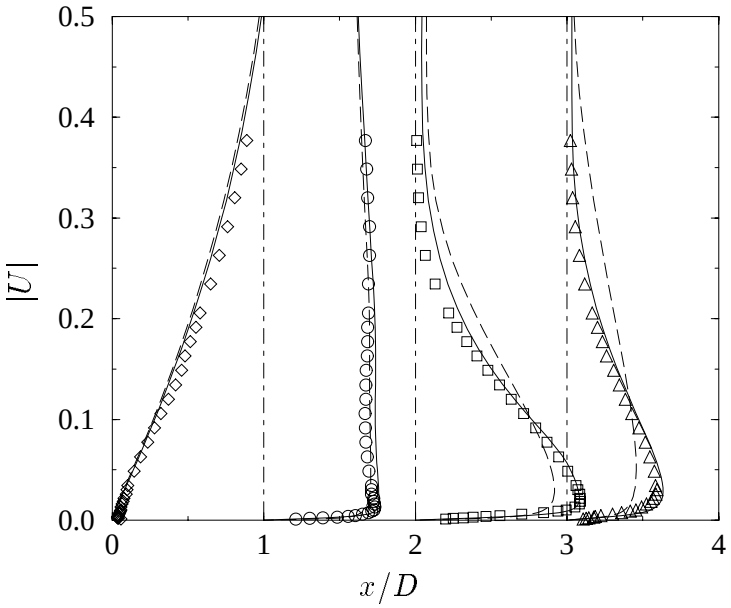

FIGURE 5. Profiles of the velocity magnitude at various radial locations [$r/D =$ 0 ($\diamond$), 0.5 ($\circ$), 1 ($\square$), 2.5 ($\triangle$)] for $H/D = 2$, experimental data (Cooper *et al.*, 1993), ——— : $k-\varepsilon-\overline{v^2}$ model, — — — : $k-\varepsilon$ model.

In the stagnation region, the spuriously high value of k predicted by the $k-\varepsilon$ model results in a significant over-prediction of the local Nusselt number as seen in Fig. 6. In this model, the stagnation Nusselt number is about 200% higher than the measured value, whereas the $k-\varepsilon-\overline{v^2}$ model prediction is only about 9% higher. Downstream of the stagnation region, the $k-\varepsilon$ Nusselt number rapidly decreases and approaches the experimental and $k-\varepsilon-\overline{v^2}$ values. The experimental data indicate a dip in the local Nusselt number distribution around $r/D = 1.4$ and a secondary maximum at around $r/D = 2$. Some investigators (e.g. Lee *et al.* 1995) have attributed the local maximum to transition from a laminar to turbulent boundary layer in the wall jet region. This is not supported by the measurements of Lytle and Webb, who note that there are relatively high levels of turbulence even in the stagnation region. It is believed that the increase in the turbulent kinetic energy away from the stagnation region (as observed by Lytle and Webb and predicted by the $k-\varepsilon-\overline{v^2}$ model), where the shear layer of the jet directly interacts with the flat plate, is responsible for this local increase of the Nusselt number. It appears that the data of Yan indicate a more pronounced local minimum of Nusselt number

compared to the data of Baughn. Also, in the data of Yan, this point is shifted closer to the stagnation point with a somewhat lower lower value of the local Nusselt number in the region of $r/D < 1.5$. The $k-\varepsilon-\overline{v^2}$ model does not predict a local secondary maximum; however, it does show a deflection in the local Nusselt number distribution. It can be said that the agreement between the data and the $k-\varepsilon-\overline{v^2}$ computation is excellent in the regions of $r/D \leq 1$ and $r/D \geq 1.8$.

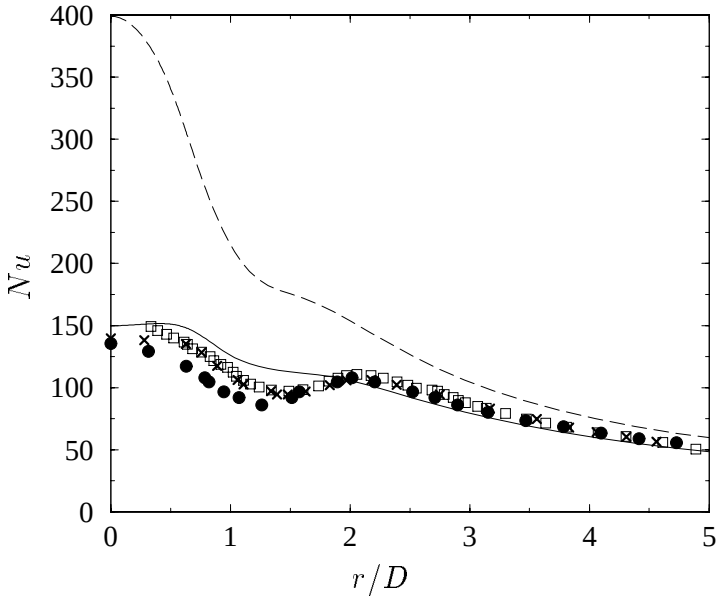

FIGURE 6. Distribution of local wall heat transfer coefficient for $H/D = 2$, ——— : $k-\varepsilon-\overline{v^2}$ model, – – – : $k-\varepsilon$ model, experimental data (for symbol key see Fig. 2).

2.4.3 Results for $H/D = 6$

The contours of the turbulent kinetic energy are shown in Fig. 7. The maximum value of k predicted by the $k-\varepsilon$ model is 66% higher than $k-\varepsilon-\overline{v^2}$. The location of this maximum, shown by the arrows on this figure, is in the stagnation region for the $k-\varepsilon$, and at about $r/D = 1$ for the $k-\varepsilon-\overline{v^2}$.

A comparison of the predicted and measured local Nusselt number is presented in Fig. 8. It is noted that in the impingement region there is a 25% scatter in the experimentally measured Nusselt number. The data of Lytle and Webb is consistently higher than measurements of others. The $k-\varepsilon$ model over-predicts the stagnation Nusselt number by about 150%, but the discrepancy gradually reduces, moving away from the impingement region. The $k-\varepsilon-\overline{v^2}$ model prediction is in excellent agreement with the data of Lytle and Webb in the impingement region; however, in the wall jet region there is better agreement with the data of Yan. It is noted that unlike the lower aspect ratio results ($H/D = 2$), there is no secondary maximum in the Nusselt number distribution. This is believed to be attributed to the fact that as the jet is moved further out from the impingement surface, the location of maximum k moves closer to the jet axis. This is supported by the

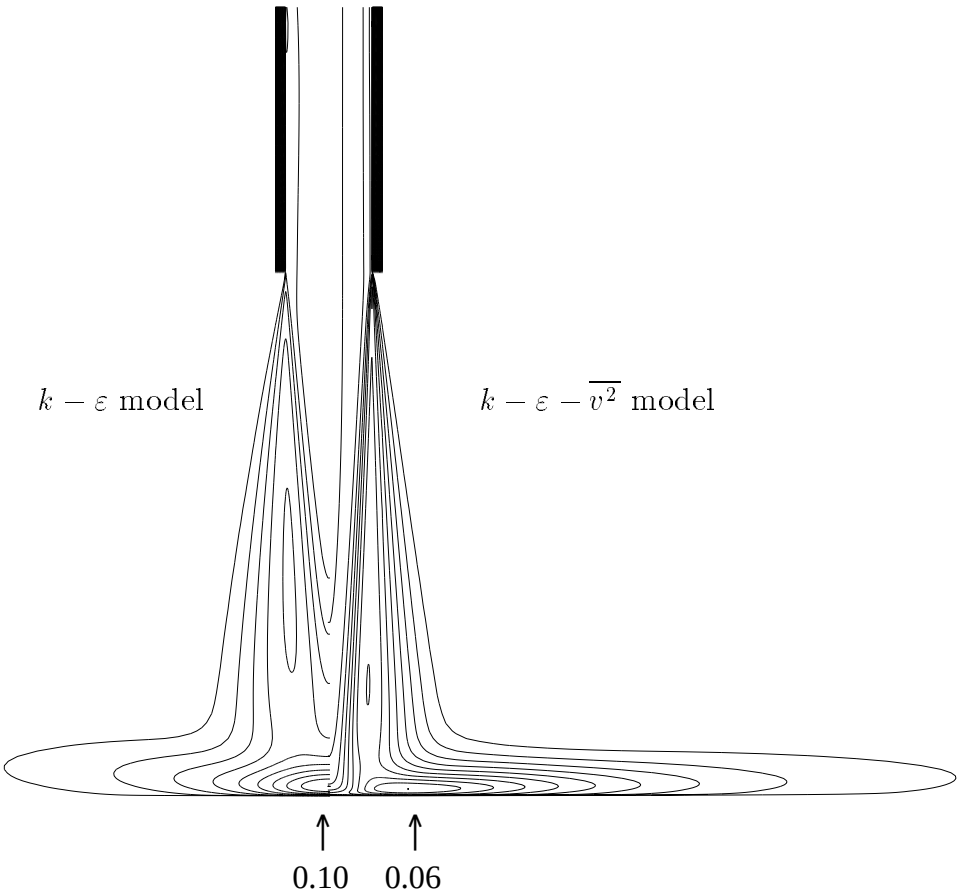

FIGURE 7. Contours of turbulent kinetic energy for $H/D = 6$.

computations with the $k-\varepsilon-\overline{v^2}$ model, which predicts the location of this point at r/D of 2 and 1 for aspect ratios of 2 and 6, respectively.

2.4.4 Stagnation Nusselt number

Simulations have been carried out for a constant Reynolds number ($Re_D = 23,000$) and a wide range of aspect ratios ($0.5 \leq H/D \leq 14$) to determine the dependence of the stagnation Nusselt number on H/D. This dependence is crucial to many applications of impingement cooling. A comparison of the computed values with the experimental data is presented in Fig. 9. The $k-\varepsilon-\overline{v^2}$ model predictions are in good agreement with the data. Also, experimental measurements (e.g. Baughn and Shimizu 1989, Yan 1993 and Lee *et al.* 1995) have indicated that for $H/D > 1$, the stagnation Nusselt number exhibits a maximum value at around $H/D = 6$. Our $k-\varepsilon-\overline{v^2}$ computations confirm this finding and indicate that the maximum stagnation Nusselt number is between H/D of 6 and 7. This is attributed to the increase in the turbulent kinetic energy as the jet is moved away from the impingement surface. For instance, as previously discussed, the maximum of k at $H/D = 6$ is higher than that of $H/D = 2$. This is also supported by Kataoka *et al.* (1987), who show that turbulent intensity reaches a maximum at an aspect ratio of 7. The measurements of Lytle and Webb also indicate that at lower spacing ratios,

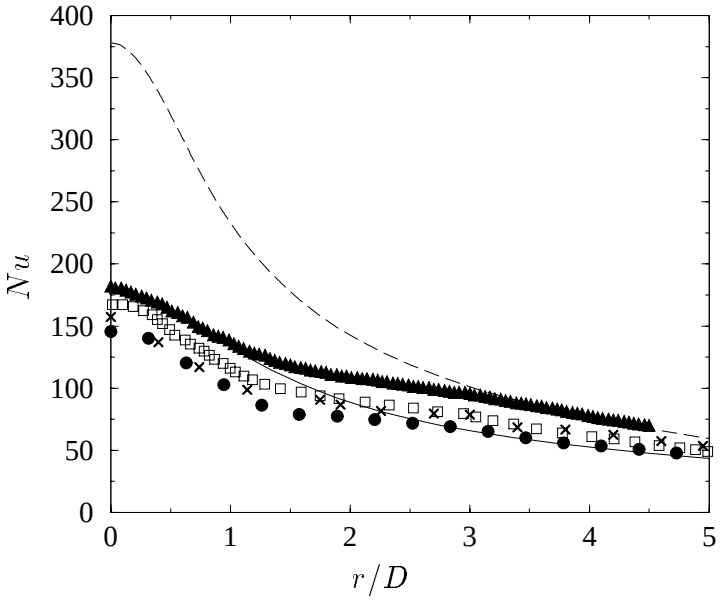

FIGURE 8. Distribution of local wall heat transfer coefficient for $H/D = 6$, ——— : $k-\varepsilon-\overline{v^2}$ model, — — — : $k-\varepsilon$ model, experimental data (for symbol key see Fig. 2).

the stagnation Nusselt number goes through a local minimum at $H/D = 1$, which is also correctly predicted by the $k-\varepsilon-\overline{v^2}$ model.

The $k-\varepsilon$ model substantially over-predicts the stagnation Nusselt number. It also indicates a behavior unlike the trend observed in the experiments and the $k-\varepsilon-\overline{v^2}$ computations. Two local maxima around H/D of 3 and 5 with a local minimum around 4 are noted. At higher aspect ratios, the $k-\varepsilon$ predictions gradually approach the measurements.

3. Future plans

The main aim of this research has been to accurately and economically predict the heat transfer rate in an impinging jet. The computations carried out to date have shown that the $k-\varepsilon-\overline{v^2}$ model predictions agree very well with the experiments, whereas the $k-\varepsilon$ model, in general, does not properly resolve the flow features, highly over-predicts the rate of heat transfer, and yields physically unrealistic behaviors.

It is planned to perform additional two- and three-dimensional computations to cover a wider range of parameters, such as the geometry, Reynolds number, and Prandtl number. In particular, for electronic cooling applications, dielectric liquids in a confined jet geometry need to be explored. There are also some recently obtained experimental measurements of heat transfer from a heated pedestal being cooled by an impinging jet which will be used for comparison with future simulations. The understanding gained and the obtained results can be directly relevant to the design and operation of a number of industrial and engineering applications.

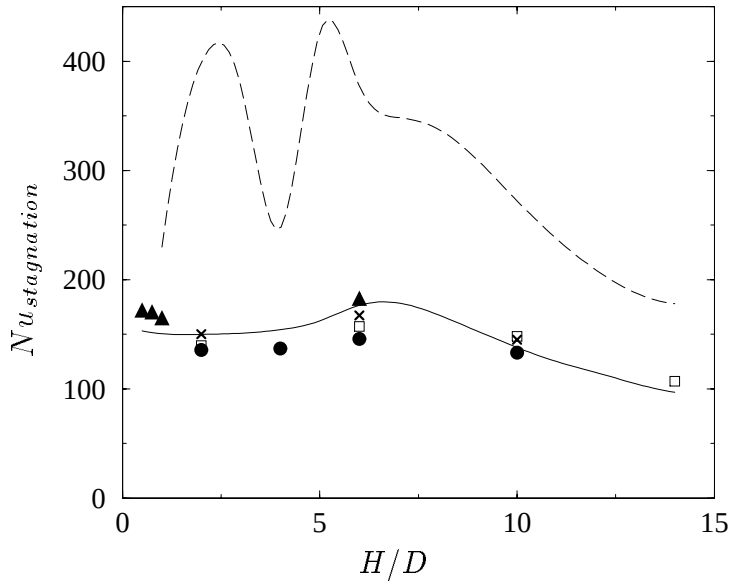

FIGURE 9. Effect of jet distance on the heat transfer at the stagnation point, ——— : $k-\varepsilon-\overline{v^2}$ model, – – – : $k-\varepsilon$ model, experimental data (for symbol key see Fig. 2).

Acknowledgments

We thank Profs. Baughn (UC, Davis), Webb (BYU), and Yan (Southern Illinois) for providing their experimental data.

REFERENCES

BAUGHN, J., HECHANOVA, A. & YAN, X. 1991 An experimental study of entrainment effects on the heat transfer from a flat surface to a heated circular impinging jet. *J. Heat Transfer.* **113,** 1023-1025.

BAUGHN, J. & SHIMIZU, S. 1989 Heat transfer measurements from a surface with uniform heat flux and an impinging jet. *J. Heat Transfer.* **111,** 1096-1098.

COOPER, D., JACKSON, D., LAUNDER, B. & LIAO, G. 1993 Impinging jet studies for turbulence model assessment–I. Flow-field experiments. *Int. J. Heat Mass Transfer.* **36** (10), 2675-2684.

CRAFT, T., GRAHAM, L. & LAUNDER, B. 1993 Impinging jet studies for turbulence model assessment–II. An examination of the performance of four turbulence models. *Int. J. Heat Mass Transfer.* **36** (10), 2685-2697.

DURBIN, P. 1991 Near-wall turbulence closure without damping functions. *Theoretical & Comp Fluid Dyn.* **3** (1), 1-13.

DURBIN, P. 1993a A Reynolds-stress model for near-wall turbulence. *J. Fluid Mech.* **249,** 465-498.

DURBIN, P. 1993b Application of a near-wall turbulence model to boundary layers and heat transfer. *Int. J. Heat & Fluid Flow.* **14** (4), 316-323.

DURBIN, P. 1995 Separated flow computations with the $k-\varepsilon-\overline{v^2}$ model. *AIAA J.* **33** (4), 659-664.

DURBIN, P. 1996 On the $k-\varepsilon$ stagnation point anomaly. *Int. J. Heat & Fluid Flow.* **17,** 89-90.

ERCOFTAC DATABASE 1996 data obtained from http://fluindigo.mech.surrey.ac.uk/.

KATAOKA, K., SUGURO, M., DEGAWA, K., MARUO, K. & MIHATA, I. 1987 The effect of surface renewal due to large-scale eddies on jet impingement heat transfer. *Int. J. Heat Mass Transfer.* **30,** 559-567.

KAYS, W. M. 1994 Turbulent Prandtl number - Where are we? *J. Heat Transfer.* **116,** 284-295.

KIM, J.& MOIN, P. 1987 Transport of passive scalars in a turbulent channel flow. *Proceedings of 6th international symposium on turbulent shear flows,* Toulouse, France, September 7-9, 5.2.1-5.2.6.

LEE, D., GREIF, R., LEE, S. & LEE, J. 1995 Heat transfer from a flat plate to a fully developed axisymmetric impinging jet. *J. Heat Transfer.* **117,** 772-776.

LYTLE, D. 1990 Air jet impingement heat transfer at low nozzle-to-plate spacings. *MS Thesis,* Brigham Young University.

LYTLE, D. & WEBB, B. 1994 Air jet impingement heat transfer at low nozzle-plate spacings. *Int. J. Heat Mass Transfer.* **37**(2), 1687-1697.

NAKAYAMA, W. 1995 Heat transfer engineering in systems integration: outlook for closer coupling of thermal and electrical designs of computers. *IEEE Transactions on Components, Packaging, and Manufacturing Technology-Part A.* **18**(8), 818-826.

YAN, X. 1993 A preheated-wall transient method using liquid crystals for the measurement of heat transfer on external surfaces and in ducts. *Ph.D. Thesis,* University of California, Davis.